Journal of Physics Communications

OPEN ACCESS

RECEIVED
11 August 2019

REVISED
13 October 2019

ACCEPTED FOR PUBLICATION
29 October 2019

PUBLISHED
27 January 2020

PAPER

Numerical solution of micropolar nanofluids with Soret, Dufor effects and multiple slip conditions

Wubshet Ibrahim[1] **and Chaluma Zemedu**

Department of Mathematics, Ambo University, Ambo, Ethiopia
[1] Author to whom any correspondence should be addressed.

E-mail: wubshetib@yahoo.com **and** chalumaz48@gmail.com

Keywords: three dimensional boundary layer flow, dufour and soret effect, micro-polar nano fluid, stretching sheet, multi-slip conditions

Abstract

The objective of this study is to explore the effects of Dufour and Soret with multiple slip conditions on 3D boundary layer flow of a micropolar nanofluid. The mathematical modeling for the flow problem has been created. Using appropriate similarity transformation and non-dimensional variable, the governing non-linear boundary value problem is reduced to a coupled high order non-linear ordinary differential equations which is numerically solved. The solutions were using method bvp4c from matlab software for different quantities of governing parameters. The influences of different parameters on skin friction coefficients $(-f''(0),\ -g''(0))$, wall duo stress coefficients $(-\phi_1'(0),\ -\phi_2'(0))$ the Nusselt number $-\theta'(0)$, Sherwood number $-s'(0)$ as well as the velocities, temperature, and concentration are examined and discussed through tables and graphs. The finding results indicate the skin friction coefficients, wall duo stresses coefficients (along both x- and y-axes), the Nusselt number and the Sherwood number demonstrate decreasing behavior for an increase in slip parameters but the opposite effects are detected with the values of stretching ratio parameters. A comparison with previous studies available in the literature has been done and a very good agreement is obtained.

Nomenclature

A, B	velocity slip constants
a, b	stretching constants (s^{-1})
$C_{f(xz)}$, $C_{f(yz)}$	Skin friction coefficient
c_p	specific heat ($JKg^{-1}K^{-1}$)
c_s	concentration susceptibility
C	concentration
C_∞	ambient concentration
C_w	wall concentration
C_{slip}	concentration slip
d	solutal slip constant
D_B	Brownian diffusion coefficient (m^2s^{-1})
D_f	Dufour number
D_{CT}	Soret-type diffusion coeff.
D_T	Thermophoretic diffusion coeff.
D_{TC}	Dufour-type diffusion coefficient
f′, g′	dimensionless velocity
f, g	dimensionless stream functions

h	thermal slip constant
D	first order solutal slip parameter
H	first order thermal slip
D_m	mass diffusion (m^2s^{-1})
V	velocity of the fluid (ms^{-1})
U	the characteristic of velocity (ms^{-1})
L	the characteristic of length (m)
j	micro-inertia density (m^2)
K	thermal conductivity ($Wm^{-1}K^{-1}$)
n	microrotation parameter
Re_x, Re_y	local Reynolds numbers
s	dimensionless concentration
M_{xz}, M_{yz}	wall couple stresses coeff. (m^2s^{-1})
N_2, N_1	micro rotations at surface (s^{-1})
N_b	Brownian motion parameter
N^*_1, N^*_2	micro rotations in boundary layer
N_t	thermophoresis parameter
Nu_x	local Nusselt number
Pr	Prandtl number
q_w, q_m	heat and mass fluxes (Wm^{-2}, Kgm^2s)
Sc	Schmidt number
Sh_x	Sherwood number
Sr	Soret number
T	temperature of the fluid (K)
T_w	wall temperature (K)
T_∞	ambient temperature (K)
T_k	thermal diffusion ratio (m^2s^{-1}})
T_m	fluid mean temperature (K)
T_{slip}	temperature slip at the surface
u, v, w	velocity components (ms^{-1})
u_{slip}, v_{slip}	velocities slip
x, y, z	Cartesian coordinates

Greeks

λ	stretching rate parameter
β	material parameter
α	first order slip parameter
η	dimensionless similarity variable
θ	dimensionless temperature
ϕ_1, ϕ_2	dimensionless angular velocity
δ	boundary layer thickness(m)
μ	coefficient of dynamic viscosity(Pas)
κ	vortex viscosity coefficient (Pas)
ν	kinematic viscosity (m^2s^{-1})
ψ_x, ψ_y	stream functions (m^2s^{-1})
ρ	fluid density$($Kgm^{-3}$)
ν_s	spin -gradient viscosity ($m^2s^{-1)}$
τ_w	wall shear stress (pa)

Subscripts

∞	Conditions at the free stream
w	Condition at the surface

1. Introduction

Eringen [1] is a pioneer in conceptualization of the magnificent non-Newtonian fluid called micropolar fluid in the history of fluid dynamics. Then after two years, Eringen [2] himself has developed the ground-breaking theory on micropolar fluid. Using this theory, the mathematical model of many non- Newtonian fluids were developed for which the convectional Navier–Stokes theory unable determines it.

Following that, the computation of microplar fluid has received considerable attentions by different researches in the area of fluid dynamics. Accordingly, Xinhui *et al* [3] have examined the boundary layer flow of microplar fluid past expanding/contracting wall with porosity. Furthermore, Uddin and Kumar [4], Kucaba [5] and Ali and Alam [6] have analyzed the flow of microplar fluid under the conditions such as magnetic field, thermo diffusion and diffusion thermo and hall effect past a surface in different shape such as wedge, stretching sheet and other. Moreover, Noor *et al* [7] have computed the effect of density variation on microplar fluid with nonzero velocity slip condition. Furthermore, Haque *et al* [8] have examined the influences of viscous dissipation, Haartmann effect, convection, and joule heating on the flow of microplarfluid.

Alam *et al* [9] discussed the influence of time variation, second order slip flow, convective heating over a porous wedge with contracting or expanding characteristics. The result their study shows that the slip velocity parameter considerable affects the flow field.

Also, Nabwey *et al* [10] have presented the analysis of non-Newtonian nanofluid with the combined effect of natural and free convection flow past a vertically aligned extensible surface. The result signifies that Brownian motion and thermophoresis parameters pay a great role in deterring heat transfer rate at the surface. Moreover, Rasool *et al* [11] have examined the contribution of Laurenth force, chemical reaction and thermal radiation on the flow of nanofluid with Marangoni convective condition. Further, Rasool *et al* [12] studied the Marangoni and magnetic field effect on non-Newtonian nanofluid. The results indicate that Marangoni ratio significantly reduces the velocity profiles.

Subhakar and Gangadhar [13] have discussed the importance of thermo-diffusion, diffusion thermo and heat generation/suction on the flow Newtonian fluid. The result of the study reflects that heat source enhances the velocity and temperature of the flow. The outcomes of the study signify that Dufour and Soret numbers are to raise the skin friction.

Similarly, the effects of Dufour and Soret were reported on different papers by (EI-Kabeir *et al* [14], Chamkha and Rashad [15], Rashad and Chamkha [16], EL-Kabeir *et al* [17] and Al-Mudhaf *et al* [18]. It was found that an enhancement in the Dufour number produced a reduction in the local Nusselt number but boosts the local Sherwood number. However, the opposite behavior was predicted as Soret number raised for which the local Nusselt number was enlarged while the local Sherwood number was reduced. Hayat *et al* [19] have examined the 3D flow of couple stress fluid with effects of chemical reaction and time variation over a stretching sheet.

Sumitra [20] and Rashad *et al* [21] also reported the problem of mixed convection heat and mass transfer near an exponentially stretching surface in combination with magnetic flied, and Soret and Dufour effects. It was found that increasing material parameter resulted in enhancement of all the skin friction coefficient, Nusselt and Sherwood numbers. Moreover, Ravi *et al* [22] presented the effects of time variation and buoyance force on convective flow of micropolar fluid. It is indicated that vortex viscosity, material parameter and Prandtl number have a significant impact on flow field. The problem of heat and mass transfer on MHD boundary layer flow over a moving a vertical porous plate with suction, Soret and Dufour effects is investigated by Srinivasa *et al* [23].

Moreover, Uddin *et al* [24] addressed the impact of various physical parameters such as viscous and joule heating, multiple wall slip phenomena, mass diffusivity, variable viscosity, thermal conductivity in porous media. Furthermore, RamReddy *et al* [25] analyzed the effects of soret parameter on mixed convection flow along a vertical plate in nanofluid under the convective boundary conditions. Also Award and Sibanda [26] studied the effects of the Dufour and Soret numbers on the heat and mass transfer on a micropolar fluid through a horizontal channel.

Ibrahim [27] and Ibrahim [28] presented the investigation on micropolar fluid taking into account various determing parameters like Hartmann number, second order slip and passive control of nanoparticles. The results designated that the flow field and the engineering aspects of the study are sturdily affected by slip and material parameters.

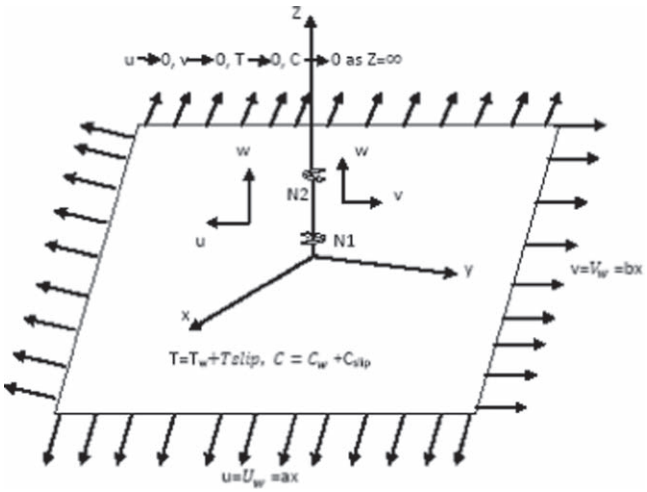

Figure 1. The flow diagram.

Rahman [29] and Ishak *et al* [30] have examined the boundary layer flow of micropolar fluid over isothermal surface in the presence thermal radiation, viscous dissipation and Joule heating. Further, the examination of micropolar fluid on bi-directional stretching surface has been carried out by Ali *et al* [31] and Ahmad *et al* [32]. The result shows that the boundary layer configuration is significantly affected by the material parameter.

The above cited research papers have discussed the flow over a plane, a vertical stretching surface, with MHD boundary flow in other area. In this paper, we study numerically the combined effects of Dufour, Soret and multiple slip conditions on three dimensional boundary layer flows to ward stretching sheet in micropolar nanofluid, using bvp4c from matlab. The effects of physical parameters on fluid velocity, skin friction coefficients, microrotation, wall couple stresses, temperature, Nusselt number, Sherwood number and concentration were considered and shown in graphs and tables as well.

2. Mathematical formulation

Consider a steady, laminar, three dimensional boundary layer flow of a viscous, incompressible micro polar nanofluid past a stretching sheet with Soret, Dufour effects, and multiple slip conditions. The fluid, which occupies a semi-infinite domain bounded by an infinite surface remains in rest. Presumed the flat surface is stretched in two lateral directions. The sheet is stretched in such a way that, the stretching velocity $u_w(x) = ax$ along x-z plane, $v_w(x) = by$ along y-z plane and $w = 0$. The flow is limited to $z \geqslant 0$. The induced first- order slips flow at the wall are given by U_{slip},V_{slip}, T_{slip} and C_{slip}. The wall temperature $T_w = T_\infty + \Delta T$. Similarly, the wall concentration, $C_w = C_\infty + \Delta C$. Where a, $b > 0$, ΔT and ΔC are constants. The harmonized frame chosen in such that x-z and y-z planes are extending along the extending sheet and z-axis is normal to them as shown in figure 1 below.

Following Ziaul *et al* [13], Ali *et al* [32] and Ahmad *et al* [33] the governing equations of boundary layer flow can be defined as:

$$\frac{\partial u}{\partial x} + \frac{\partial v}{\partial y} + \frac{\partial w}{\partial z} = 0 \tag{1}$$

$$u\frac{\partial u}{\partial x} + v\frac{\partial u}{\partial y} + w\frac{\partial u}{\partial z} = \left(\frac{\mu + \kappa}{\rho}\right)\frac{\partial^2 u}{\partial z^2} - \frac{kN_2^*}{\rho \partial z} \tag{2}$$

$$u\frac{\partial v}{\partial x} + v\frac{\partial v}{\partial y} + w\frac{\partial v}{\partial z} = \left(\frac{\mu + \kappa}{\rho}\right)\frac{\partial^2 v}{\partial z^2} + \frac{kN_1^*}{\rho \partial z} \tag{3}$$

$$u\frac{\partial N_1^*}{\partial x} + v\frac{\partial N_1^*}{\partial y} + w\frac{\partial N_1^*}{\partial z} = -\frac{\kappa}{\rho j}\left(2N_1^* + \frac{\partial v}{\partial z}\right) + \frac{v_s}{\rho j}\frac{\partial^2 N_1^*}{\partial z^2} \tag{4}$$

$$u\frac{\partial N_2^*}{\partial x} + v\frac{\partial N_2^*}{\partial y} + w\frac{\partial N_2^*}{\partial z} = -\frac{\kappa}{\rho j}\left(2N_2^* - \frac{\partial u}{\partial z}\right) + \frac{v_s}{\rho j}\frac{\partial^2 N_2^*}{\partial z^2} \tag{5}$$

$$u\frac{\partial T}{\partial x} + v\frac{\partial T}{\partial y} + w\frac{\partial T}{\partial z} = \frac{K}{\rho c_p}\frac{\partial^2 T}{\partial z^2} + \frac{D_T C_T K}{C_s C_p}\frac{\partial^2 C}{\partial z^2} + YD_B\frac{\partial C}{\partial z}\frac{\partial T}{\partial z} + \frac{YD_T}{T_\infty}\left(\frac{\partial T}{\partial z}\right)^2 \tag{6}$$

$$u\frac{\partial C}{\partial x} + v\frac{\partial C}{\partial y} + w\frac{\partial C}{\partial z} = \frac{K}{\rho c_p}\frac{\partial^2 C}{\partial z^2} + D_B\frac{\partial^2 C}{\partial z^2} + \frac{D_{CT}T_k}{T_m}\frac{\partial^2 T}{\partial z^2} + \frac{D_T}{T_\infty}\frac{\partial^2 T}{\partial z^2} \tag{7}$$

The boundary conditions at the surface and far from the plate appropriate to the flow are defined as:

$$\begin{aligned} &u = u_w + U_{slip},\ v = v_w + V_{slip},\ w = 0,\ T = T_w + T_{slip},\ C = C_w + C_{slip},\\ &N_2 = n\frac{\partial u}{\partial z},\ N_1 = -n\frac{\partial v}{\partial z}\ \ at\ \ z = 0\\ &u \to 0,\ v \to 0,\ N_1 \to 0,\ N_2 \to 0,\ T \to 0,\ C \to 0,\ as\ \ z \to \infty \end{aligned} \tag{8}$$

Where u, v and w are velocity components along the x-, y- and z-axes, correspondingly; ρ represents the fluid density; T and C are the fluid temperature and the species concentration, $\Delta T = T_w - T_\infty$ is change of temperature, $\Delta C = C_w - C_\infty$ is change in concentration. μ is dynamic coefficient viscosity, $N^*{}_1$ and $N^*{}_2$ stand for the components of the microrotation vector N normal to the planes x-z, and y-z in that order. $j = \frac{\nu}{a}$ is the microinertia density, κ stands for coefficient of vortex viscosity, K is thermal conductivity, $v_s = \left(\mu + \frac{k}{2}\right)j = \nu\left(1 + \frac{\beta}{2}\right)j$, represents the microrotation(the spin gradient) viscosity, β is the material parameter, $\Upsilon = \frac{\rho c_p}{\rho c_f}$ is the ratio between the effective heat capacity of the nano particle material and the heat capacity of the fluid, D_B and D_T stand for the Brownian and the thermophoretic diffusion coefficient respectively, c_p, c_s, T_K, T_m are specific heat capacity at constant pressure, the concentration susceptibility, the thermal -diffusion ratio,and the fluid mean temperature, correspondingly, D_{TC} and D_{CT} represent the Dufour and the Soret-type diffusivity, in that order.

U_w, V_w, are wall velocity along x-, and y-axes, respectively, N_1, N_2 stand wall microrotations x-, and y- axes, in that order, n is microrotation parameter which is constant such that $0 \leqslant n \leqslant 1$. When $n = 0$ that is, $N_1 = N_2 = 0$, the flow particle concentration is strong in which the microelements closed to the wall surface are unable to go around. When $n = \frac{1}{2}$, the anti-symmetric part of the stress tensor is vanishing which means weak concentration whilst the case $n = 1$ is used for developing the turbulent boundary layer flows.

Following Noor *et al* [8] and Uddin *et al* [25], the U_{slip}, V_{slip} velocities and the T_{slip} temperature, C_{slip} concentration beside the stretching surfaces at the wall presented and defined as:

$$\begin{aligned} &U_{slip} = \alpha_w\left((\mu + k)\frac{\partial u}{\partial z} + kN_2\right),\ V_{slip} = \alpha_w\left((\mu + k)\frac{\partial v}{\partial z} + kN_1\right),\\ &T_{slip} = h\frac{\partial T}{\partial z},\ C_{slip} = d\frac{\partial C}{\partial z} \end{aligned} \tag{9}$$

where, α_w is the dimensional slips along stretching surfaces, h and d are constants.

The similarity variable is defined by:

$$\eta = z\sqrt{\frac{a}{\nu}} \tag{10}$$

The dimensionless variables f, g, ϕ_1, ϕ_2, θ, s are introduced as:

$$\begin{aligned} &f(\eta) = \sqrt{\frac{\psi_x}{\nu\,\mathrm{Re}_x}},\ g(\eta) = \sqrt{\frac{\psi_y}{\nu\,\mathrm{Re}_y}},\ \theta(\eta) = \frac{T - T_\infty}{T_w - T_\infty},\ s(\eta) = \frac{C - C_\infty}{C_w - C_\infty},\\ &\phi_1(\eta) = \frac{N_1^*}{N_1},\ \phi_2 = \frac{N_2^*}{N_2} \end{aligned} \tag{11}$$

The equation of continuity is satisfied if the we choose a stream function $\psi(x, y)$ such that

$$u = \frac{\partial \psi}{\partial y},\ v = -\frac{\partial \psi}{\partial x} \tag{12}$$

By means of the above similarity transformation and dimensionless variables, the main equations (2)–(7) are reduced into the ordinary differential equations as follow:

$$(1 + \beta)f''' + f''(f + g) - (f')^2\beta\phi_2' = 0 \tag{13}$$

$$(1 + \beta)g''' + g''(f + g) - (g')^2\beta\phi_1' = 0 \tag{14}$$

$$\left(1 + \frac{\beta}{2}\right)\phi''_1 + (f + g)\phi_1' - \beta(g'' + 2\phi_1) - g'\phi_1 = 0 \tag{15}$$

$$\left(1 + \frac{\beta}{2}\right)\phi''_2 + (f + g)\phi_2' - \beta(f'' + 2\phi_2) - f'\phi_2 = 0 \tag{16}$$

$$\frac{1}{\mathrm{Pr}}\theta'' + D_f s'' + (f+g)\theta' + Nbs'\theta' + Nt(\theta')^2 = 0 \tag{17}$$

$$\frac{1}{Sc}s'' + S_r\theta'' + \frac{1}{S_c}\frac{Nt}{Nb}\theta'' + (f+g)s' = 0 \tag{18}$$

With the boundary conditions:

$$\begin{aligned}
&\eta = 0, f(0) = 0, g(0) = 0, g'(0) = Bg''(0), f'(0)\\
&= \quad Af''(0), \phi_2(0) = nf''(0), \phi_1(0) = -ng''(0),\\
&\theta(0) = 1 + H\theta'(0), s(0) = 1 + Ds'(0),\\
&\eta \to \infty, f'(\infty) \to 0, g'(\infty) \to 0, \phi_2(\infty) \to 0,\\
&\phi_1(\infty) \to 0, \theta(\infty) \to 0, s(\infty) \to 0
\end{aligned} \tag{19}$$

Here the governing parameters are defined by:

$$\begin{aligned}
&D_f = \frac{D_{TC}T_k}{c_s c_p}\frac{C_w - C_\infty}{T_w - T_\infty}, \mathrm{Pr} = \frac{\rho\nu c_p}{K}, S_r = \frac{D_{TC}T_k}{T_m\nu}\frac{T_w - T_\infty}{C_w - C_\infty},\\
&Sc = \frac{\nu}{D_B}, Nb = \frac{(\rho_c)_p}{(\rho_c)_f}\frac{D_B}{\nu}(C_w - C_\infty)\\
&A = 1 + \alpha(1 + (1+n)\beta), B = 1 + \alpha(1 + (1-n)\beta),\\
&Nt = \frac{(\rho_c)_p}{(\rho_c)_f}\frac{D_T}{T_\infty\nu}(T_w - T_\infty)
\end{aligned} \tag{20}$$

Where f and g are the dimensionless stream functions along the x- and *y*-axis respectively, f′ and g′ stand for the dimensionless velocities, ϕ_1, ϕ_2, θ and s, the component of angular velocity along x-and y-axes, temperature, and concentration correspondingly. η is the similarity variable, the primes (“,”,’) show differentiation with respect to η. The Prandtl number, Pr, gives a measure of relative value of momentum and heat transport by diffusion in the velocity and thermal boundary layers, correspondingly. The value $\mathrm{Pr} = 2$ indicates that the relative growth of velocity boundary layer is twice the growth of the thermal boundary layer. D_f, Sr, Sc, Nb, and Nt represent the Dufour number, the Soret number, the Schmidt number, the Brownian motion parameter, and the thermophoresis parameter in that order.

The engineering quantities of curiosity in this study are skin friction coefficients, Nusselt and Sherwood numbers, wall couple stresses M_{zx} and M_{zy}. These can be defined as:

$$C_{fxz} = \frac{\tau_{xz}}{\rho u_w^2}, C_{fyz} = \frac{\tau_{yz}}{\rho u_w^2}, Nu_x = \frac{xq_w}{k(T_w - T_\infty)}, Sh_x = \frac{xq_m}{D_B(C_w - C_\infty)}, M_{zx} = \frac{m_w}{\rho u_w^2}$$

$$\tau_{xz} = \left((\mu + k)\frac{\partial u}{\partial z} + kN_2\right)_{z=0}, \tau_{yz} = \left((\mu + k)\frac{\partial v}{\partial z} + kN_1\right)_{z=0}, q_w = -K\left(\frac{\partial T}{\partial z}\right)_{z=0}$$

where

$$q_m = -D_B\left(\frac{\partial C}{\partial z}\right)_{z=0}, m_w = \nu_s\left(\frac{\partial N_2}{\partial z}\right)_{z=0}, m_w = \nu_s\left(\frac{\partial N_1}{\partial z}\right)_{z=0}$$

Using the above equations, we get:

$$\begin{aligned}
&C_{fxz}\frac{(\mathrm{Re}_x)^{1/2}}{(1 + \beta(1+n))} = f''(0), C_{fyz}\left(\frac{x}{y}\right)\frac{(\mathrm{Re}_x)^{1/2}}{(1 + \beta(1-n))} = g''(0),\\
&M_{zx}\left(\frac{1}{(1 + 0.5\beta)\nu}\right) = \phi_2'(0), M_{zy}\left(\frac{\lambda}{(1 + 0.5\beta)\nu}\right) = \phi_1'(0),\\
&Nu_x\left(\frac{1}{(\mathrm{Re}_x)^{1/2}}\right) = -\theta'(0), Sh_x\left(\frac{1}{(\mathrm{Re}_x)^{1/2}}\right) = -s'(0)
\end{aligned} \tag{21}$$

Where

$$\begin{aligned}
&C_{fxz}\frac{(\mathrm{Re}_x)^{1/2}}{(1 + \beta(1+n))}, C_{fyz}\left(\frac{x}{y}\right)\frac{(\mathrm{Re}_x)^{1/2}}{(1 + \beta(1-n))},\\
&M_{zx}\left(\frac{1}{(1 + 0.5\beta)\nu}\right), M_{zy}\left(\frac{\lambda}{(1 + 0.5\beta)\nu}\right),\\
&Nu_x\left(\frac{1}{(\mathrm{Re}_x)^{1/2}}\right), Sh_x\left(\frac{1}{(\mathrm{Re}_x)^{1/2}}\right), \mathrm{Re}_x
\end{aligned}$$

are skin friction coefficients, wall couple stresses coefficients, Nusselt number, Sherwood number and local Reynolds, respectively.

3. Numerical solution

The coupled six harmonized high order ordinary differential equations (13)–(18), subjected to the boundary conditions, equation (19), are explained numerically using the function bvp4c from matlab software for different values of physical parameters, namely slip parameters (A, B, D, H), Prandtl number Pr, Dufour number Df, Soret number Sr, Brownian motion parameter Nb, thermophoresis parameter Nt, Schmidt number Sc, stretching ratio parameter λ, material parameter β and micro rotation parameter n. Numerical results are found using Matlab BVP solver bvp4c from matlab which is a finite difference code that applies the three- stage Lobatto IIIa formula. To apply bvp4c from matlab: equations (13)–(18) are converted into a system of first-order equations.

Second, set up a boundary value problem (bvp) and use the bvp solver in matlab to numerically solve this system, with the above boundary condition and take on a suitable finite value for the far field boundary condition, that is, $\eta \to \infty$, say $\eta_\infty = 50$. The step-size is taken as $\Delta\eta = 0.01$ and accuracy to the fifth decimal place as the measure of convergence. In solving the BVP by using matlab, bvp4c has only three arguments: a function ODEs for calculation of the residual in the boundary conditions, and a structure solint that provides a guess for a mesh. The ODEs are handled exactly as in the Matlab IVP solvers. Further clarification on the procedure of bvp4c is found in the book by Shampine *et al* [33]

Letting $y = [f\ f'\ f''\ g\ g'\ g''\ \phi\ \phi_1{}'\ \phi_2\ \phi_2{}'\ \theta\ \theta'\ s\ s\ ]^T$ gives

$$\frac{d}{d\eta}\begin{pmatrix} y(1)\\ y(2)\\ y(3)\\ y(4)\\ y(5)\\ y(6)\\ y(7)\\ y(8)\\ y(8)\\ y(10)\\ y(11)\\ y(12)\\ y(13)\\ y(14)\end{pmatrix} =$$

$$\begin{pmatrix} y(2)\\ y(3)\\ \dfrac{(y(2)\,{}_*y(2)(y(1)+y(4))_*y(3)+\beta y(10))}{(1+K)}\\ y(5)\\ y(6)\\ \dfrac{(y(5)\,{}_*y(5)(y(1)+y(4))_*y(6)-\beta y(8))}{(1+k)}\\ y(8)\\ \dfrac{(-(y(1)+y(4))y(7)+y(5)y(7)+\beta(2\,y(7)+y(6)))}{(1+0.5_*K)}\\ y(10)\\ \dfrac{(-(y(1)+y(4))y(10)+y(2)y(9)+\beta(2\,y(9)\text{-}y(3)))}{(1+0.5_*K)}\\ y(12)\\ \dfrac{(-\mathrm{PrDfSc}((y(1)+y(4))_*y(12)-\mathrm{Pr}((y(1)+y(4))y(12)+\mathrm{Nb}\,y(14)\,{}_*y(12)+\mathrm{Nt}\,y(12)^2)))}{\left(1+\mathrm{Pr\,Df}\left(-\mathrm{Sc}\left(\mathrm{Sr}+(1/Sc)\left(\frac{Nt}{Nb}\right)\right)\right)\right)}\\ y(14)\\ \dfrac{-\mathrm{Sc}\left(\left(\mathrm{Sr}+\left(\frac{1}{Sc}\right)\left(\frac{Nt}{Nb}\right)\right)(-\mathrm{PrDfSc}((y(1)+y(4))_*y(12)-\mathrm{Pr}((y(1)+y(4))_*y(12)+\mathrm{Nb}\,y(14)y(12)+\mathrm{Nt}\,y(12)2\right)}{\left(1+\mathrm{Pr\,Df}\left(-\mathrm{Sc}\left(\mathrm{Sr}+(1/Sc)\left(\frac{Nt}{Nb}\right)\right)\right)\right)+(y(1)+y(4))y(14))}\end{pmatrix} \tag{22}$$

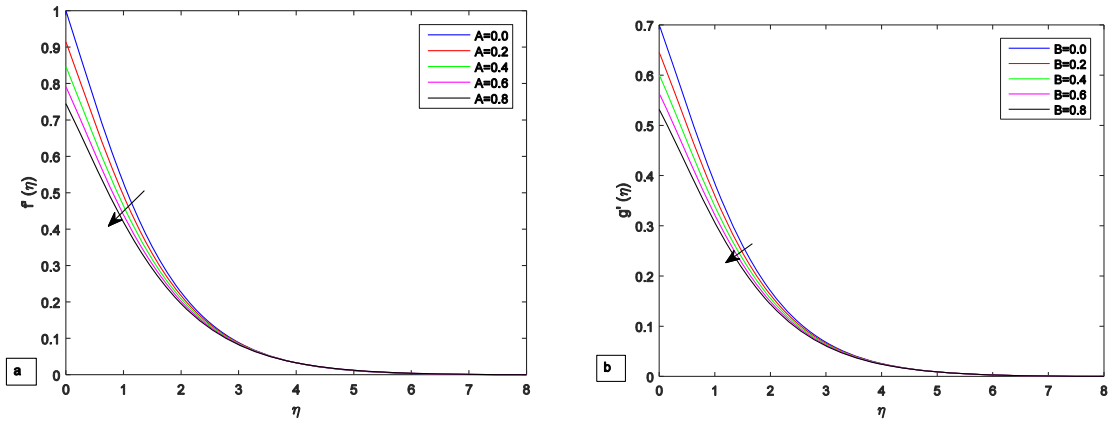

Figure 2. Graph (a) velocity profile graph f′(η) and (b) velocity profile graph g′(η) for different values of A, and B, respectively when $H = n = D = D_f = Nt = Nb = 0.5$, $\beta = \Pr = Sc = 2$, $S_r = 0.2$, $\lambda = 0.7$.

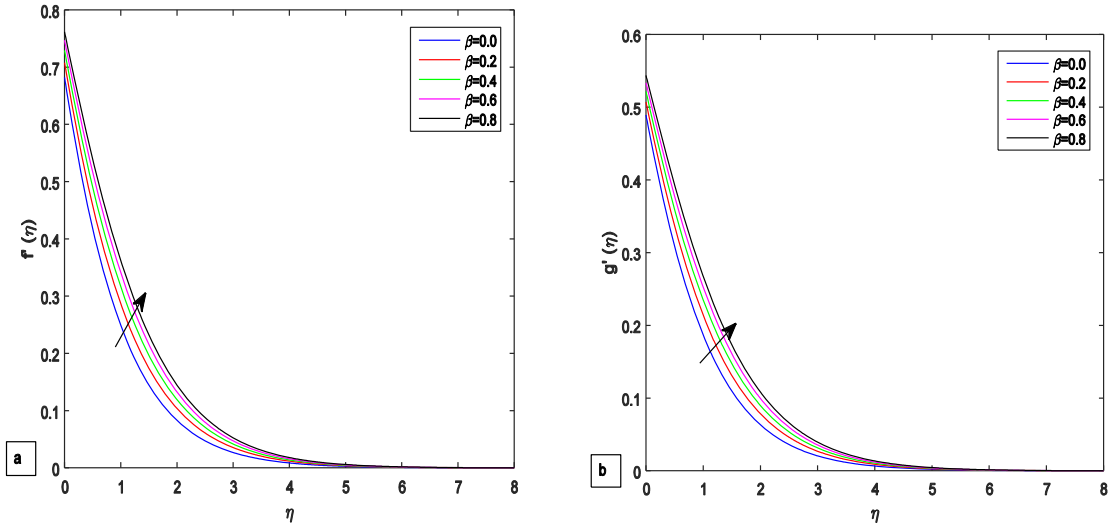

Figure 3. Graph (a) velocity profile graph f′(η) and (b) velocity profile graph g′(η) for different values of β when A = B = H = n = D = Df = Nt = Nb = 0.5, Pr = Sc = 2, Sr = 0.2, $\lambda = 0.7$.

4. Results and discussion

In this section, the influences of various governing physical parameters on non-dimensional velocities, temperature, concentration, microrotations, skin friction coefficients, wall couple stress coefficients, local heat and mass transfer rates have been considered.

4.1. Velocity profiles

The dimensionless velocity profile graphs of f′(η) and g′(η) for different values of the first order slip parameters A, B, stretching ratio λ and material parameter β are represented in figures 2–4. Figure 2 illustrates that an increase in values of slip parameters (A or B), causes a reduction in the fluid velocity profiles. However, figure 3 shows that rise in the magnitude of material parameters β, reduces the viscosity of the fluid flow that results increase in the velocity boundary layer thicknesses. Next, figure 4 reveals that an enlargement in the values of stretching ratio parameters λ, upsurge the fluid velocity g′(η). On the other hand, an enhancement in the magnitude of stretching ratio parameter λ, results in reduction of the velocity boundary layer thickness along x axis.

4.2. Angular (micro rotation) profiles

Figures 5, 6 show the upshots of material parameter β and microrotation parameter n on an angular velocity ϕ_1 (η) and ϕ_2 (η). Figure 5 indicates that arises in the quantities of β, reduce the absolute values of the angular

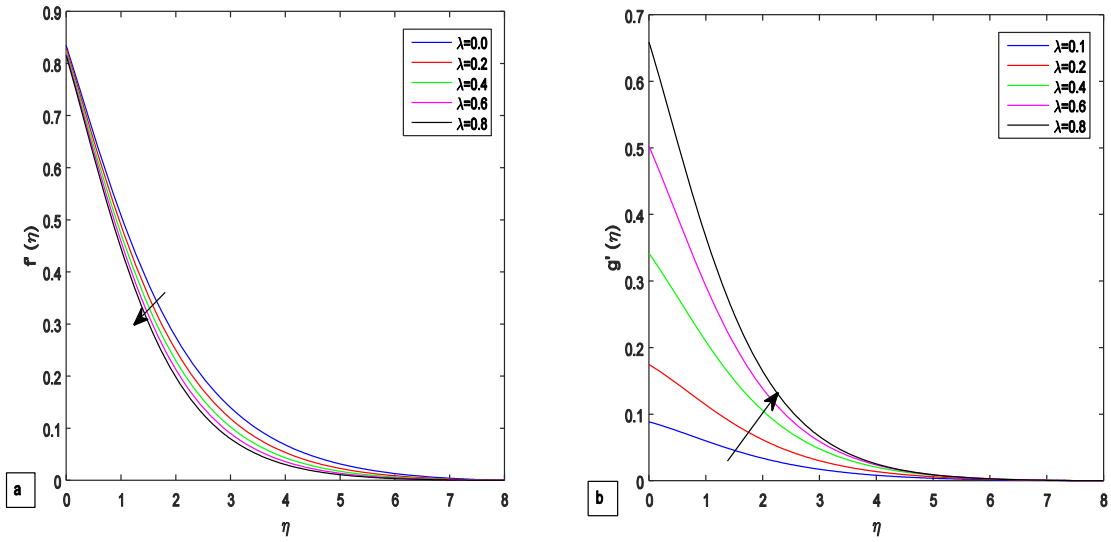

Figure 4. Graph (a) velocity profile graph $f'(\eta)$ and (b) velocity profile graph $g'(\eta)$ for different values of λ when A = B = H = n = D = Df = Nt = Nb = 0.5, β = Pr = Sc = 2, Sr = 0.2.

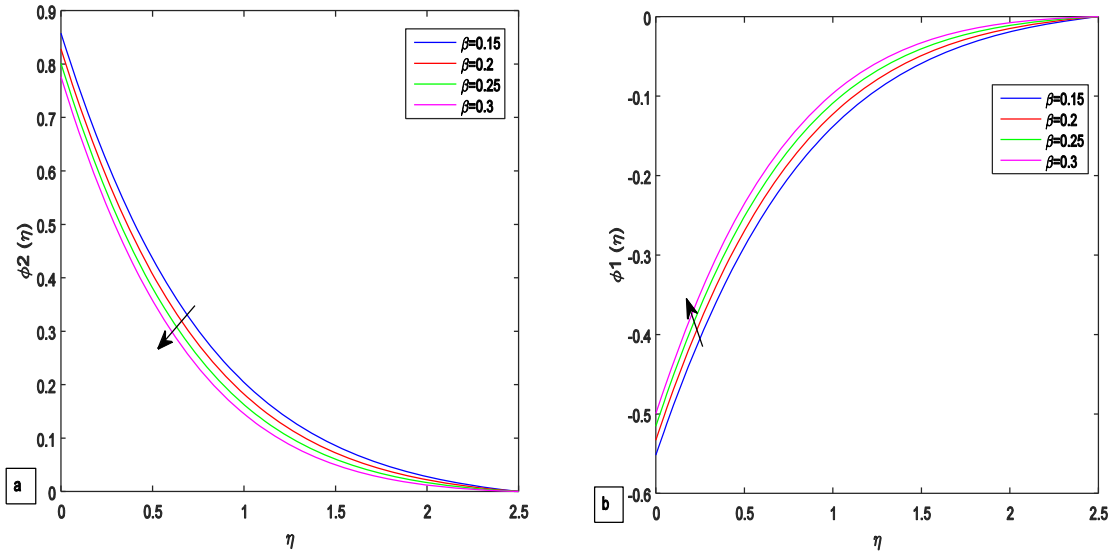

Figure 5. Graph (a) angular profile graph $\phi_2(\eta)$ and (b) angular profile graph $\phi_1(\eta)$ for different values of β when A = B = H = Df = D = Nb = Nt = 0.5, n = 1.0, Sc = Pr = 2, Sr = 0.2, λ = 0.7.

velocities. These effects occur due to the fact that an increase in the values of material limitation, raise the vortex viscosity of the fluid that causes the above effects. However, figure 6 shows that rise in the values of microrotation parameter, falls the resistance to rotate the fluid that results raise the absolute values of angular velocities.

4.3. Temperature profiles

The consequences of the slip parameter H, Dufour number Df, Soret number Sr, Prandtl number Pr, Brownian motion parameter Nb on temperature sketches are given in figures 7–9. Figure 7 indicates that boost in the values of slip parameter and Prandlt number, decline the Nusselt number, the temperature distribution. These effects are happen toward enhancing resistance to diffuse the temperature that causes decrease the Nusselt number, temperature dissemination. However, figure 8 show that as values of Dufour number, Soret number grow, result in reducing the kinematic viscosity (or increasing the thermal conductivity) of the fluid which causes increase thermal boundary layer thicknesses as shown in figure 8 (a), and by same reasoning, it correlate with decrease Nusselt number plus its boundary layer thicknesses, figure 8 (b). Moreover, figure 9 illustrates that grow in the amount of Brownian motion constraint, drop the kinematic viscosity (or enhance the Brownian

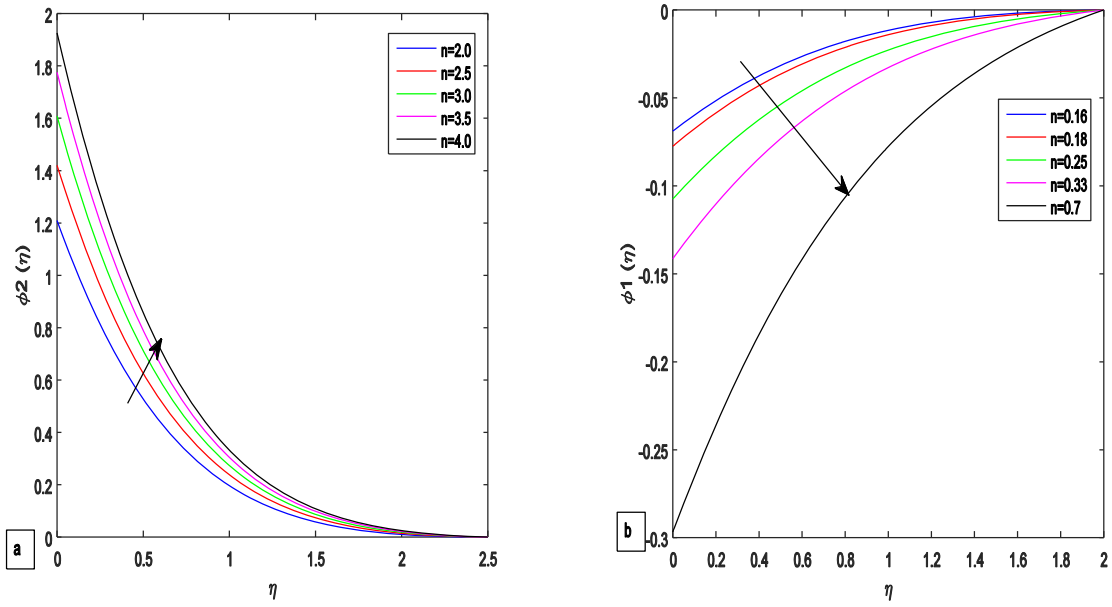

Figure 6. Graph (a) angular profile graph $\phi_2(\eta)$ and (b) angular profile graph $\phi_1(\eta)$ for different values of n when A = B = H = D = Df = Nb = Nt = 0.5, β = Pr = Sc = 2, Sr = 0.2, λ = 0.7.

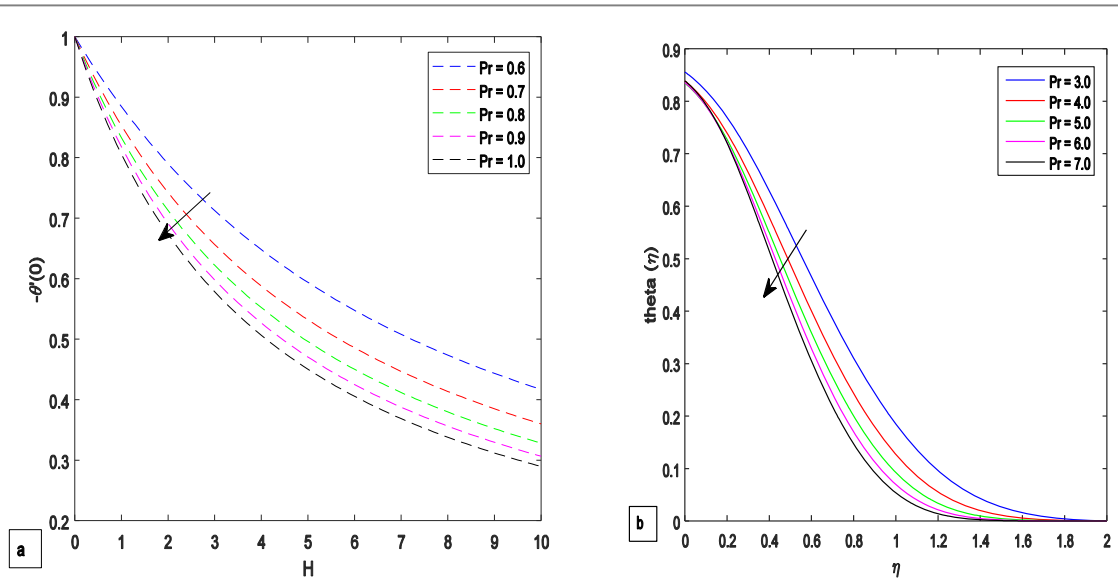

Figure 7. Graph (a) Nusselt number $\theta'(0)$ and (b) temperature profile graph θ for different values of Pr when A = B = D = n = Nb = 0.1, β = Df = Sr = Sc = Nt = 0.5, λ = 0.7 and when A = B = n = D = Df = Nt = Nb = 0.5, β = Sc = 2, Sr = 0.2, respectively

diffusion coefficient) of the fluid and resistance to diffuse the temperature that decrease in temperature profile and Nusselt number.

4.4. Concentration profiles

Figures 10, 11 show the result of different values of slip parameter D, Dufour number Df, Soret number Sr and Schmidt number Sc on concentration graph. From figure 10 it can be seen that increase in the values of D or Sc, decrease the concentration distributions with their boundary layer thicknesses. These effects are happen toward enlarge in the kinematic viscosity (or decrease in the Brownian diffusion coefficient ratio) of the fluid that causes increase the Sherwood number. Moreover, figure 11 shows that as the values of Dufour and Soret numbers grow, drop the kinematic viscosity (or enhance thermal conductivity) of the fluid result increase in Sherwood number.

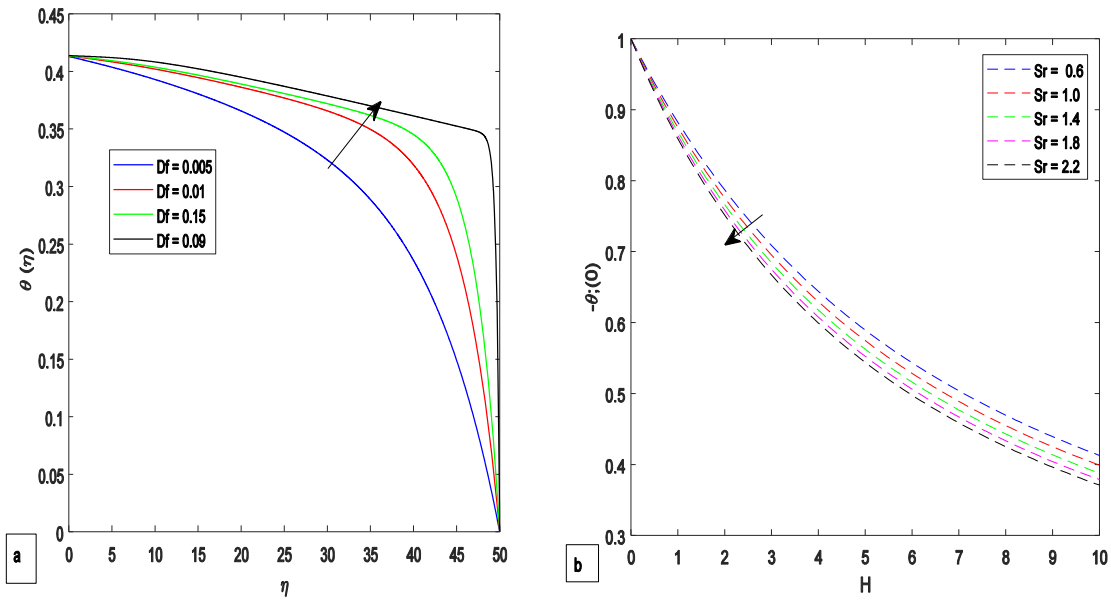

Figure 8. Graph (a) temperature profile θ and (b) Nusselt number -θ'(0) graph for different values of Df and Sr when A = B = H = n = D = Nt = Nb = 0.5, β = Pr = Sc = 2, λ = 0.7 and when A = B = D = n = Nb = 0.1, Pr = 0.6, β = Df = Sc = Nt = 0.5

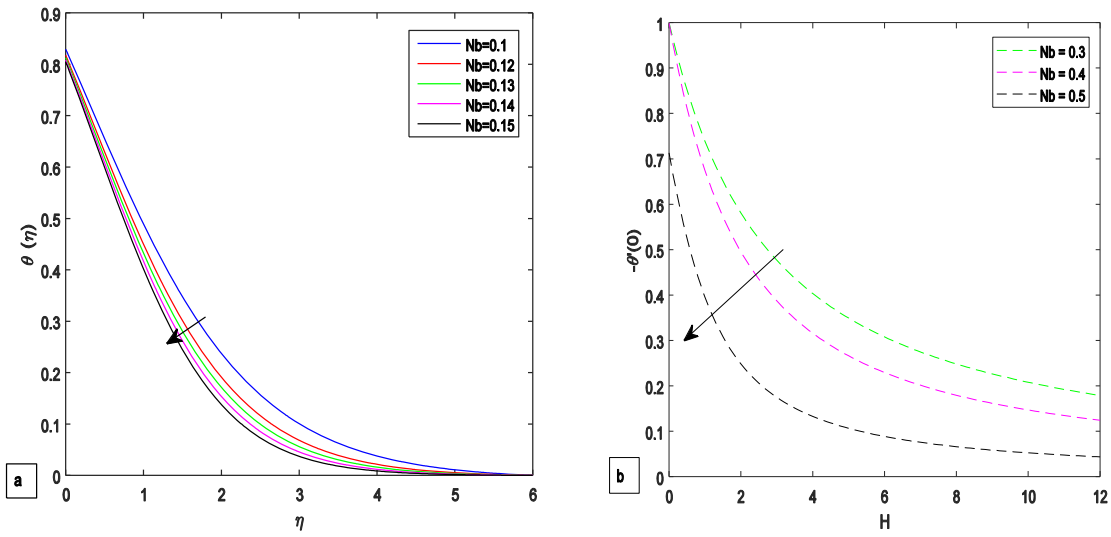

Figure 9. Graph (a) temperature profile graph and (b) Nusselt number $-\theta'(0)$ graph for different values of Nb when A = B = H = n = D = Df = Nt = 0.5, β = Pr = Sc = 2, Sr = 0.2, λ = 0.7 and whenA = B = D = n = 0. β = 0.5, Sc = 0.2

4.5. Skin frictions

Table 1 drawn to assess the exactness of the method used association with previously presented data feasible in the literature has been made. From table 1, it can be seen that the numerical values of the skin friction coefficients, $-f''(0)$, $-g''(0)$ and the wall couple coefficients $-\phi_1'(0)$, $-\phi_2'(0)$ in this paper for various values of β and λ when n = 0 is in an excellent agreement with the pervious outcomes of published paper by Ali J [31]. The outcomes indicate that the numerical used in the report is appropriate and highly accurate.

Table 2 points out that an increase in values of slip parameters (A and B), causes reduction in the skin friction coefficients along both axes. Moreover, as the magnitudes of material β and microrotation parameters n increase, reduces opposition to flow the fluid that results reduction of skin friction coefficients. However, an increase in the magnitude of stretching ratio parameter λ, results an increase in the values of skin friction coefficients along both axes.

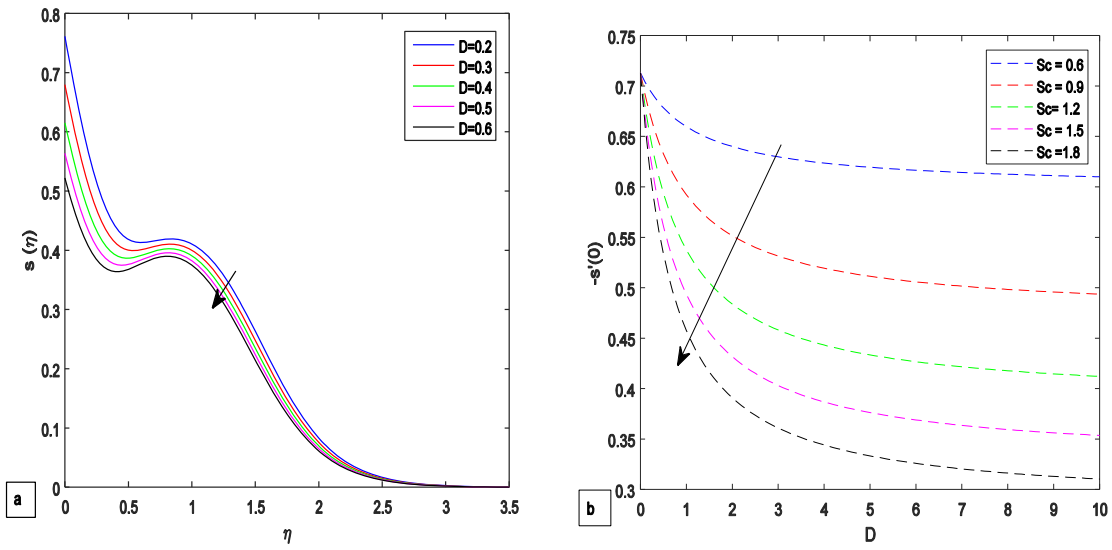

Figure 10. Graph (a)concentration profiles and (b) Sherwood number-s(0) graph for different values of D and Sc when A = B = H = n = 0.5, β = Pr = 2, and when A = B = H = n =0.1, λ = 0.7, Sr = 0.2, β = Df = Nb = Nt = 0.5

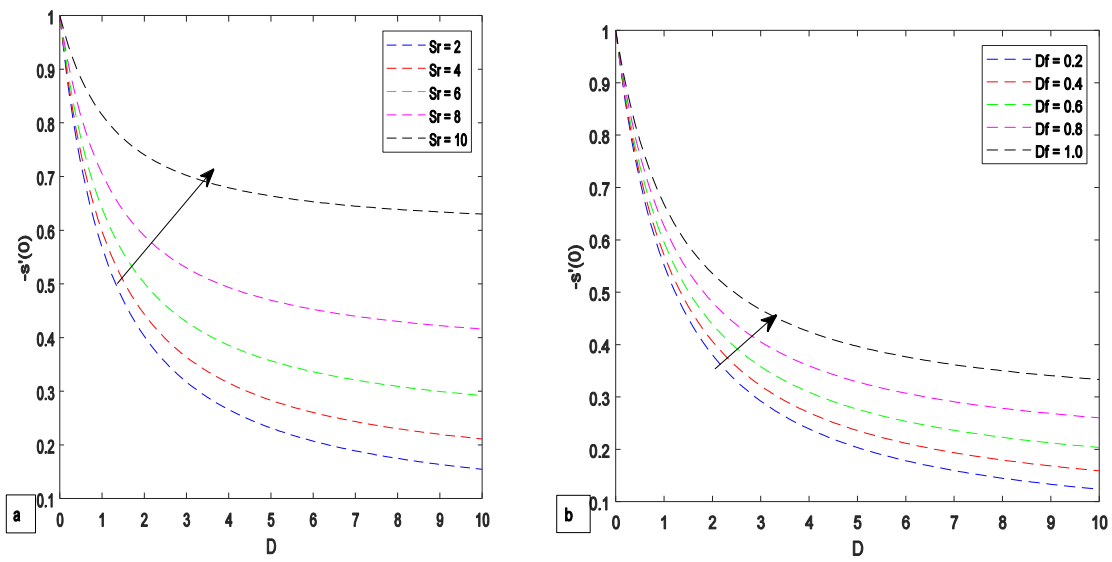

Figure 11. Graph (a) and (b) Sherwood number-s(0) graph for different values of Df and Sr respectively when $A = B = H = n = 0.1$, $\lambda = 0.7$, $Pr = 0.6$, $\beta = Nb = Sc = Nt = 0.5$.

Table 1. Comparison of skin friction coefficients $-f'(0)$ and $-g'(0)$, $-\phi_1(0)$, $\phi_2(0)$, when n = 0 for different values of β and λ with previously published result.

present result						Ali J [31]			
β	λ	$-f'(0)$	$-g'(0)$	$-\phi_1'(0)$	$-\phi_2'(0)$	$-f'(0)$	$-g'(0)$	$-\phi_1'(0)$	$-\phi_2'(0)$
0.0	0.0	1.0000	0.0000	0.000	0.0000	1.0000	0.0000	0.000	0.0000
0.0	0.25	1.0487	0.1945	0.000	0.000	1.0493	0.1947	0.000	0.000
0.0	0.5	1.0929	0.4651	0.000	0.000	1.0931	0.4653	0.000	0.000
0.0	0.75	1.1343	0.7945	0.000	0.000	1.1348	0.7945	0.000	0.000
0.0	1.0	1.1735	1.1735	0.000	0.000	1.1740	1.0740	0.000	0.000
0.5	1.0	0.9481	0.9481	0.2011	0.2011	0.9482	0.9482	0.2012	0.2012
1.0	1.0	0.8080	0.8080	0.2831	0.2831	0.8083	0.8083	0.2833	0.2833
2.0	1.0	0.6410	0.6410	0.3403	0.3403	0.6410	0.6410	0.3405	0.3405
3.0	1.0	0.5427	0.5427	0.3510	0.3510	0.5430	0.5430	0.3513	0.3513

Table 2. The computed values of skin friction coefficients -f′(0) and $-g'(0)$, $-\phi_1(0)$, $\phi_2(0)$, Nusselt number $\theta'(0)$, Sherwood number s′(0) when H = D = Nb = Nt = Df = 0.5, Pr = 2, Sc = Sr = 0.2 for different values of A, B, n, β and λ.

A	B	β	λ	N	$-f'(0)$	$g'(0)$	$-\phi_1(0)$	$\phi_2(0)$	$\theta'(0)$	$S'(0)$
0.4	0.5	0.2	0.7	0.5	0.3835	0.2387	0.3542	0.5570	0.5812	0.1369
0.6	0.5	0.2	0.7	0.5	0.3480	0.2365	0.3505	0.5069	0.5714	0.1338
0.8	0.5	0.2	0.7	0.5	0.3192	0.2345	0.3473	0.4660	0.5628	0.1310
0.5	0.2	0.2	0.7	0.5	0.3681	0.2740	0.4045	0.5363	0.5872	0.1385
0.5	0.4	0.2	0.7	0.5	0.3658	0.2484	0.3679	0.5323	0.5795	0.1363
0.5	0.6	0.2	0.7	0.5	0.3639	0.2277	0.3381	0.5290	0.5729	0.1344
0.5	0.8	0.2	0.7	0.5	0.3622	0.2104	0.3134	0.5261	0.5672	0.1327
0.5	0.5	0.0	0.7	0.5	0.6360	0.4216	0.1817	0.2966	0.5413	0.2005
0.5	0.5	0.5	0.7	0.5	0.5225	0.3439	0.3081	0.4702	0.5625	0.1815
0.5	0.5	1.5	0.7	0.5	0.4016	0.2621	0.3523	0.5311	0.5748	0.1494
0.5	0.5	2.0	0.0	0.5	0.3311	0.0000	0.000	0.4717	0.4467	0.0909
0.5	0.5	2.0	0.3	0.5	0.3470	0.0823	0.1267	0.4997	0.5124	0.1153
0.5	0.5	2.0	0.7	0.5	0.3648	0.1548	0.3523	0.5306	0.5761	0.1353
0.5	0.5	2.0	1.0	0.5	0.3766	0.2375	0.5508	0.5508	0.6139	0.1451
0.5	0.5	2.0	0.7	0.0	0.4257	0.2788	0.1654	0.2379	0.5667	0.1421
0.5	0.5	2.0	0.7	0.2	0.3989	0.2666	0.2470	0.3653	0.5709	0.1391
0.5	0.5	2.0	0.7	0.4	0.3755	0.2447	0.3192	0.4785	0.5745	0.1365

Table 3. The computed values of Nusselt number-θ'(0) and Sherwood number s′(0) when A = B=n = Nt = Nb = Df = 0.5, Pr = β = 2, Sr = Sc = 0.2, λ = 0.7 for different values of H, D, Nt, Sr, Pr, Df, Nb and Sc

H	D	Nt	Pr	Df	$-\theta'(0)$	$s'(0)$
0.5	0.5	0.5	2.0	0.5	0.5761	−0.1353
1.0	0.5	0.5	2.0	0.5	0.4743	−0.0742
1.5	0.5	0.5	2.0	0.5	0.3951	−0.0229
0.5	0.0	0.5	2.0	0.5	0.5978	−0.1786
0.5	0.5	0.5	2.0	0.5	0.5761	−0.1353
0.5	1.0	0.5	2.0	0.5	0.5631	−0.1093
0.5	2.0	0.5	2.0	0.5	0.5482	−0.0793
0.5	0.5	0.5	2.0	0.5	0.5761	−0.1353
0.5	0.5	0.6	2.0	0.5	0.4060	−0.0550
0.5	0.5	0.7	2.0	0.5	0.3183	−0.0075
0.5	0.5	0.5	1.0	0.5	0.1307	0.2472
0.5	0.5	0.5	1.5	0.5	0.0138	0.4125
0.5	0.5	0.5	1.6	0.5	0.0016	0.4579
0.5	0.5	0.5	2.0	0.1	0.0011	0.3867
0.5	0.5	0.5	2.0	0.2	0.0032	0.3662
0.5	0.5	0.5	2.0	0.3	0.0060	0.3510

4.6. Wall couple stresses

Table 2 illustrates that an increase in values of slip parameters (A and B), causes reduction in wall couple stress coefficients along both axes. However, rise in the magnitudes of material parameter β, drops the viscosity of the fluid flow that results increase(it upsurge the values of) in wall couple stress coefficients along both axes. Moreover, an increase in the values of stretching ratio parameter λ, results boost in wall couple stress coefficients nearby both axes.

4.7. Nusselt number

Table 2 indicates that an enhancement in quantities of slip parameters (A and B), causes reduction in the Nusselt number. However, rise in the magnitude of material parameters β and microrotation n, drops the viscosity of the fluid flow that results in rise the Nusselt number. What's more, an increase in the magnitude of stretching ratio parameter λ, results in rise the value of the Nusselt number.

Table 3 it can be seen that increase in the values of slip parameters (H, D) and Prandlt number, reduce the local Nusselt number. Moreover, as the absolute values of Dufour and Schmidt numbers, and thermophoresis parameter grow, result in reducing the kinematic viscosity of the fluid that causes decrease local Nusselt number.

4.8. Sherwood number

Table 2 point out that an enlargement in values of slip parameters (A and B), causes reduction in the Sherwood number. Moreover, rise in the magnitude of material parameters β and microrotation n, reduces resistance to flow the fluid that results decrease in the value of Sherwood number. However, arise in the magnitude of stretching ratio parameter λ, results in rise the value of the Sherwood number.

Table 3 it can be seen that as H and D are increasing, the absolute values of local Sherwood number is decreasing. These outcomes are happen due to the fact that fall the mass diffusion, associate in reducing the local Sherwood number. However, as the values of Df and Sc grow, drop the kinematic viscosity of the fluid results the local Sherwood number growth with Df and Sc. Moreover, boost in the amount of Prandtl number, increases resistance to diffuse the temperature that results increase in the value of local Sherwood number. On contrary, enhance in absolute value of thermphoresis parameter, causes in reduce the value of local Sherwood number.

5. Conclusions

This study considers the effects of Dufour and Soret with multiple slip conditions on three dimensional boundary layer flow of a micropolar nanofluid over a stretching sheet were discussed. The boundary layer equations of the flow problem are reduced into a twosome of high order non- linear ordinary differential equations using the similarity transformation. Then, the obtained differential equations are solved numerically using bvp4c from matlab software. Numerical results are obtained for different main parameters of the flow problem. Comparison with previously published work was performed and very good agreement was obtained. The effects of governing parameters are presented using figures and tables. The main findings are:

1. The velocity profiles reveal decreasing performance for raising values of slip parameters (A or B) while an inverse outcome is seen when material parameter β is improved.
2. The existence of the stretching parameter λ allows to decline the velocity boundary layer thickness near wall for $f'(\eta)$ and to enhance the velocity profile $g'(\eta)$ near the surface of plane.
3. The temperature profile distribution within the boundary layer can be increased by the raise in the values of Dufour number Df; but it can be decreased by the increase in either the values of prandtl number Pr or Brownian motion parameter Nb.
4. An enhancement in either the values of Prandtl number Pr or Soret number Sr or Brownian motion parameter Nb allows reducing the Nusselt number as well as its boundary layer thickness near the surface of the wall.
5. Boost in the values of solutal slip parameter D agrees to reduce concentration boundary layer thickness.
6. Sherwood number exhibits increasing behavior for improve either Soret Sr or Dufour Df number. But it exhibits opposite behavior for enhance in the values of Schmidt number Sc.
7. The skin friction coefficients $-f''(0)$ and $-g''(0)$ demonstrate decreasing behavior for the increase in either velocity slip parameters (A or B) or material parameter β or micro rotation parameter n while an inverse outcome is observed when the values of stretching parameter λ is raised.
8. The wall couple stress coefficients $-\phi_1'(0)$, $-\phi_2'(0)$ reveal declining performance for growth velocity slip parameters (either A or B) whereas opposite result is pragmatic for increase either material parameter β or microrotation parameter n or stretching parameter λ.

ORCID iDs

Wubshet Ibrahim https://orcid.org/0000-0003-2281-8842

References

[1] Ac E 1964 Simple microfluids *Intrnational journal of Engineering Science* **2** 205–17
[2] Ac E 1966 Theory of mcropolar fluids *Journal of Mathematics and Mechenics* **16** 1–8
[3] Si X, Zn L, Ping L, Zn X and Zn Y 2013 Flow and heat transfer of a micro polar fluid in a porous channel with expanding or contacting walls *Int. J. Heat Mass Transfer* **67** 885–95
[4] Uddin Z and Kumar M 2013 Hall and ion-slip effect on MHD boundary layer flow of a micro polar fluid past a wedge *Scientia Ir.* B **20** 467–76
[5] Pietal K A 2004 Micro channals flow modelling with the micro polar fluid theory *Rzeszow Poland. Tech. Sci.* **52**

[6] Ali M and ShanAlam M 2013 Soret and Dufour effects on steady free convection in MHD micro polar fluid flow, mass and heat transfer with Hall current *International journal of advancements in Research and Technology* **2** ISSN 2278-7763
[7] Noor N F M, Rizwan U I H, Nadeem S and Hashim I 2015 Mixed convection stagnation flow of a micro polar nano fluid along a vertically stretching surface with slip effects *Meccanica* **50** 2007–22
[8] Ziaul M, Md M A, Ferdows M and Postelnicu A 2012 Micro polar fluid behaviors on steady MHD free convection and mass transfer flow with constant heat and mass fluxes, joule heating and viscous dissipation *J. Eng. Sci.* **24** 71–84
[9] Alam M S, Honque M M and Uddin M J 2016 Convective flow of nano fluid along a permeable stretching or shrinking wedge with second order slip using Buongiorno's mathematical model *International Journal of Advanement in Applied Mathematics and Mechanics.* **3** 79–91
[10] Nabwey. H A, Boumazgour M and Rashad A M 2017 Group method analysis of mixed convection stsgnation- point flow of non-newtonian nanofluid over a vertical stretching surface *Indian J. Phys.* **91** 731–42
[11] Rasool Gh. Z T, Shafiq A and Durur H 2019 Infuence of chemical reaction on Marangni convective flow of nanofluid in the presence of Larntz forces and thermal radition *Journal of Advances in Nanotechnology* **1** 32–49
[12] Rasool Gh. Z T and Shafiq A 2019 Mangoni effect in second grade forced convective flow of water based nanofluid *Journal of Advances in Nanotechnology* **1** 50–61
[13] Subhakar N J and Gangadhar K 2010 Soret and Dufour effects on MHD free convection heat and mass transfer flow over a stretching vertical plate with suction and heat surce or sink *International Journal of modern Engineering Research* **2** 3458–68
[14] EI-Kabeir A S M M, Chamkha A and Rashad A M 2010 Heat and mass transfer by MHD stagnation point flow of a power-law fluid towards a streatching surface with radiation, chemical reaction and soret and dufour effects *Intarnational Journal of Chemical Reactor Engineering* **8** 1–18
[15] Chamkha Ali J and Rashad A M 2014 Unsteady heat and mass transfer by mhd mixed convection flow from a rotating vertical cone with chemical reaction and dufour and soret effects *Can. J. Chem. Eng.* **92** 758–67
[16] Rashad A and Chamkha A 2014 Heat and mass transfer by natural convection flow of about a truncated cone in porous media with soret and dufour effects *Int. J. Numer. Methods Heat Fluid Flow* **24** 595–612
[17] EL-Kabeir S M M, Modather M and Rashad A M 2015 Heat and mass transfer by unsteady natural convection over a moving vertical plate embedded in a saturated porous medium with chemical reaction, Soret and Dufor effects *Journal of Applied Fluid Mechanics* **8** 453–63
[18] Al-Mudhaf Ali F, Rashad A M, Ahmed Somel E, Chamkha Ali J and KabeirS M M E L 2018 Soret and dufour on unsteady double diffusive natural convection in porous trapezoidal enclosures *Int. J. Mech. Sci.* **140** 172–8
[19] Hayat T, Wais M, Safdar A and Hendi Au A 2012 unsteady three dimensional flow of couple stress fluid over a stretching surface with chemical reaction *Nonlinear Ana.:mo.* **17** 47–59
[20] Sumitra S 2013 Convective transport over an exponentially stretching surface *MSc Thesis* National Institute of Technology Rourkela (ODISHA) (Rourkela, India)
[21] Rashad A M, Abbasbandy S and Chamkha Ali J 2014 Mixed convection flow of micropolar fluid over a continuously moving vertical surface immersed in a thermally and solutally strratified medium with chemical reaction *J. Taiwan Inst. Chem. Eng.* **45** 2163–9
[22] Ravi S K, Singh A K, Sngh R K and Chamkha A J 2013 Transient free convective flow of a micro polar fluid between two vertical walls, Int *J. Industrial mathematics* **5** IJIM-0031 No. 2
[23] Srinivasa R G, Raana B, Rami Reddy B and Vidyasagar G 2014 Soret and Dufour effects on MHD boundary layer flow ver a moving vertical porous plate with suction *International Journal of Tr.* **2** 215–26
[24] Uddin J M, Beg Anwer O and Uddin N M 2016 Multiple slips and variable transport property effect on magnetohydromagnetic dissipative thermosolutal convection in a porous, Medium *J. Aerosp. Eng.* **29** 04016024
[25] RamReddy Ch. M P V S N, Chankha Ali J and Rashad A M 2013 The Soret effect on mixed convection flow in a nano fluid under convective boundary condition *Int. J. Heat Mass Transfer* **64** 384–92
[26] Award F and Sibanda P 2010 Dufour and Soret effects on heat and mass transfer in a micro polar fluid in a horizontal channel *WSEAS Transaction on Heat and Mass Transfer* **5** 165–77
[27] Ibrahim W 2017 MHD boundary layer flow and heat transfer of micro polar fluid past a stretching sheet with second order slip *J. Braz. Soc. Mech. Sci. Eng.* **39** 791–99
[28] Ibrahim W 2016 Passive Control of nanoparticle of micropolar fluid past a stretching sheet with nanoparticles, convective boundary condition and second -order slip *J. Process Mechanical Eng.* **0** 1–16
[29] Rahman M M 2009 Convective flow of micro polar fluids from radiate isothemal porous surfaces with viscous dissipation and Joule heating *Commun Nonlinear Sci Numer simulat.* **14** 3018–30
[30] Ishak A, Nazar R and Pop I 2006 Flow of micro polar fluid on a continuous moving surface *Warszawa Arch. Mech. 58* **6** 529–41
[31] Chama Ali J, Jaradat M and Pop I 2003 Three -dimensional micropolar flow due to a stretching flat surface. international journal of mechanics *Research* **30**
[32] Ahmad K, Nazar R, Ishak A and Pop I 2012 Unsteady three -dimensional boundary layer flow due to a stretching surface in a micro polar fluid *Int. J. Muner. Meth. Fluids* **68** 1561–73
[33] Shampine L F, Glandwell I and Thomson S 2003 *Solving ODEs with Matlab* (New York, USA: Cambridge)